Molecular Therapy
Original Article

Development of a translatable gene augmentation therapy for *CNGB1*-retinitis pigmentosa

Laurence M. Occelli,[1] Lena Zobel,[2,3] Jonathan Stoddard,[4] Johanna Wagner,[2] Nathaniel Pasmanter,[1] Janice Querubin,[1] Lauren M. Renner,[4] Rene Reynaga,[4] Paige A. Winkler,[1] Kelian Sun,[1] Luis Felipe L.P. Marinho,[1] Catherine R. O'Riordan,[5] Amy Frederick,[5] Andreas Lauer,[6] Stephen H. Tsang,[7] William W. Hauswirth,[8] Trevor J. McGill,[4,6] Martha Neuringer,[4,6] Stylianos Michalakis,[2,3] and Simon M. Petersen-Jones[1]

[1]College of Veterinary Medicine, Michigan State University, 736 Wilson Road, East Lansing, MI 48864, USA; [2]Department of Pharmacy–Center for Drug Research, Ludwig-Maximilians-Universität München, 81377 Munich, Germany; [3]Department of Ophthalmology, University Hospital, LMU Munich, 80336 Munich, Germany; [4]Oregon National Primate Research Center, Oregon Health & Science University, 505 NW 185th Avenue, Beaverton, OR 97005, USA; [5]Genomic Medicine Unit, Sanofi, 225 Second Avenue, Waltham, MA 02451, USA; [6]Casey Eye Institute, Oregon Health & Science University, 515 Campus Drive, Portland, OR 97239, USA; [7]Jonas Children's Vision Care, Departments of Ophthalmology, Pathology and Cell Biology, Institute of Human Nutrition, Columbia Stem Cell Initiative, Vagelos College of Physicians and Surgeons, New York, NY 10032, USA; [8]Department of Ophthalmology, College of Medicine, University of Florida, Box 100284 HSC, Gainesville, FL 32610, USA

In this study, we investigate a gene augmentation therapy candidate for the treatment of retinitis pigmentosa (RP) due to cyclic nucleotide-gated channel beta 1 (*CNGB1*) mutations. We use an adeno-associated virus serotype 5 with transgene under control of a novel short human rhodopsin promoter. The promoter/capsid combination drives efficient expression of a reporter gene (AAV5-RHO-eGFP) exclusively in rod photoreceptors in primate, dog, and mouse following subretinal delivery. The therapeutic vector (AAV5-RHO-CNGB1) delivered to the subretinal space of *CNGB1* mutant dogs restores rod-mediated retinal function (electroretinographic responses and vision) for at least 12 months post treatment. Immunohistochemistry shows human *CNGB1* is expressed in rod photoreceptors in the treated regions as well as restoration of expression and trafficking of the endogenous alpha subunit of the rod CNG channel required for normal channel formation. The treatment reverses abnormal accumulation of the second messenger, cyclic guanosine monophosphate, which occurs in rod photoreceptors of *CNGB1* mutant dogs, confirming formation of a functional CNG channel. *In vivo* imaging shows long-term preservation of retinal structure. In conclusion, this study establishes the long-term efficacy of subretinal delivery of AAV5-RHO-CNGB1 to rescue the disease phenotype in a canine model of *CNGB1*-RP, confirming its suitability for future clinical development.

INTRODUCTION

Gene augmentation therapy driven by adeno-associated virus (AAV) vectors is being advanced for several blinding inherited retinal degenerations (IRDs). This strategy led to the first approved commercial product, Luxturna, for the treatment of Leber congenital amaurosis due to *RPE65* mutations.[1] Several clinical trials are underway for other IRDs (see Georgiou et al. for a recent review[2]), and translational programs are developing further therapies, including the program reported here for retinitis pigmentosa (RP) due to mutations in the cyclic nucleotide-gated channel subunit beta 1 gene (*CNGB1*).

RP is an important IRD that is genetically heterogeneous, with mutations causing non-syndromic RP having been identified in 69 genes (see RetNet[3] https://web.sph.uth.edu/RetNet, accessed on Jan 17, 2023) and affecting approximately 1 in 4,000 people.[4] Biallelic mutations in *CNGB1* cause a typical RP with an initial loss of the rod cells (dim-light responsive photoreceptors that comprise about 95% of the total number of photoreceptors). Rod photoreceptor loss is followed by an inevitable and progressive loss of cone cells (brighter light responsive photoreceptors needed for color vision and good visual acuity).[5–7] *CNGB1* mutations are reported to be the sixth most prevalent cause of recessive IRD, with an estimated 109,247 affected patients world-wide.[8]

CNGB1 combines with three CNG alpha 1 (CNGA1) subunits to form a CNG channel in the cell membrane of rod photoreceptors.[9] In the dark, levels of rod outer segment cyclic guanosine monophosphate (cGMP) are higher, increasing the chances of CNG channel opening

Received 19 January 2023; accepted 10 April 2023;
https://doi.org/10.1016/j.ymthe.2023.04.005.

Correspondence: Simon M. Petersen-Jones, College of Veterinary Medicine, Michigan State University, 736 Wilson Road, East Lansing, MI 48864, USA.
E-mail: peter315@msu.edu
Correspondence: Stylianos Michalakis, Department of Ophthalmology, University Hospital, LMU Munich, 80336 Munich, Germany.
E-mail: michalakis@lmu.de

allowing cation influx, which depolarizes the cell. Following light activation of the rod phototransduction cascade, cGMP is hydrolyzed, the CNG channels close, and the rod becomes hyperpolarized, reducing neurotransmitter signaling to second-order neurons. In the absence of CNGB1, degradation of the CNGA1 subunit occurs, and the outer segments of rods are almost completely devoid of CNG channels.[10,11] Thus CNGB1 deficiency leads to a severe reduction in rod function and accumulation of cGMP, followed by a slowly progressive loss of rods and eventually secondary loss of cones. The disease phenotype shows a disconnect between loss of function and loss of structure, with an early loss of rod function and dim-light vision preceding significant loss of rod photoreceptors. This pattern and the slow loss of rods are important features providing a broad "window of opportunity" for gene augmentation therapy.[12]

Fortunately, relevant animal models are available to develop translational therapy. We have reported initial proof of concept studies in an engineered mouse and spontaneously occurring dog model of *CNGB1*-RP with a complex mutation in *CNGB1* (c.2387delA; 2389_2390insAGCTAC) that leads to skipping of exon 26 and introduction of a premature stop codon and lack of CNGB1 expression.[10,11,13,14] The next stage toward a first-in-human clinical trial is the development of a suitable construct. We have recently reported on rescue of rod function in the *Cngb1*-X26 mouse model using an AAV serotype 5 construct with human *CNGB1* cDNA driven by a novel short human rhodopsin promoter.[15] The purpose of this current study was to further evaluate the suitability of this vector for a future clinical trial by demonstrating its pharmacodynamic efficacy in a large animal model with an eye size similar to that of humans. We show that the short rhodopsin promoter drives efficient rod-specific expression in nonhuman primates as well as dogs and mice. AAV5-RHO-CNGB1 results in long-term rescue of rod function in the dog model with preservation of retinal structure and cone function. The vector is therefore a suitable candidate to advance toward a human clinical trial.

RESULTS

A short human rhodopsin promoter drives rod-specific transgene expression in nonhuman primates, dogs, and mice

The large size of the *CNGB1* cDNA (3.76 kb) requires a construct with a short rod-specific promoter to avoid exceeding the packaging limit of AAV vectors (4.7 kb). A short human rhodopsin promoter (194 bp) was designed based on the human promoter sequence.[15] As a test of the efficacy and rod specificity of transgene expression driven by this novel promoter, an expression cassette with eGFP packaged in an AAV5 capsid was delivered into the subretinal space of nonhuman primates (NHPs), mouse, and dog. Table S1 provides information about the NHP study showing the four treatment doses investigated. In the NHP eyes, three subretinal injection blebs were created surrounding the fovea. This multi-bleb approach could be modified in a human trial to target the perimacular ring of high rod density while trying to avoid detachment of the fovea, which has been reported to be potentially deleterious.[1,16,17] In all three species, expression of eGFP was detected on fluorescent fundus imaging *in vivo* by 1 month post injection (PI) (Figures 1 and S1A–S1C). The NHPs were euthanized 3 months after injection and eyes processed for immunohistochemistry (IHC) and tissues collected for biodistribution studies. The eyes from the injected mice and dogs were also processed for IHC. In all three species, IHC of frozen retinal sections showed eGFP expression in the injected retinal regions (Figures 1, S1D, and S1E). Importantly, this was only present in rod photoreceptors (appearing in the entire cell length). The NHP study showed a clear dose effect (Figures 1B and 1C) with a significant correlation between eGFP expressing rods per unit length of retinal section and dose used (Welch's one-way ANOVA, $F(3, 1.93) = 122.29$, $p = 0.009$). IHC using rod and cone markers showed eGFP expression was specific to rods and with no expression detected in cones or any other retinal cell type (Figure 2 for NHP, Figures S1D and S1E for dog and mouse).

A biodistribution study analyzing a variety of tissues (Table S2 lists tissues sampled) from the injected NHPs only detected the vector genome in one repeat sample of a single optic nerve (animal 1 OD, dose group 1); all other samples were negative.

Gene augmentation using AAV5-RHO-CNGB1 restores CNG channel formation, reversing toxic accumulation of cGMP

IHC showed that *CNGB1* transgene was exclusively expressed in rod photoreceptors in the treated regions of the *CNGB1*-mutant dogs (Figures 3 and S2–S4). Treatment also resulted in rescue of the endogenous partner channel subunit (CNGA1) from degradation. In the treated region, but not the untreated, CNGA1 protein was detectable in rod outer segments, suggesting formation of chimeric canine CNGA1:human CNGB1 channels. There appeared to be some effect of dosage on strength of expression of the *CNGB1* transgene as shown by the representative sections in Figure 3, but this was a subjective assessment.

A feature of lack of CNG channel function in rod outer segments is the abnormal accumulation of cGMP. IHC showed that this was reversed within the treated retinal regions (Figure 4), while in the same eyes, cGMP could still be detected within the photoreceptors in the untreated regions. We noted that on many sections of the treated retinal regions, CNGB1 was detected throughout the rod cells in addition to the outer segments, which is the functional site of CNGB1. It was noticeable that with lower transgene expression toward the edge of the treatment bleb, CNGB1 was only present in outer segments (Figure S4).

Gene augmentation using AAV5-RHO-CNGB1 rescues rod function in the *CNGB1* dog model

Using ten 3-month-old *CNGB1* mutant dogs, a dose-escalation study with four treatment groups (Gp1–Gp4) was performed (Table 1). Two subretinal injections were given in each treated eye (blebs resulting from subretinal injections can be seen on the immediate post-injection fundus images in the first column of Figure 3). Two eyes were untreated and acted as controls (Gp0). For statistical analysis only, electroretinography (ERG) and vision testing results from four additional untreated age-matched *CNGB1*-mutant dogs from previous studies were included with the results from the two Gp0 animals to

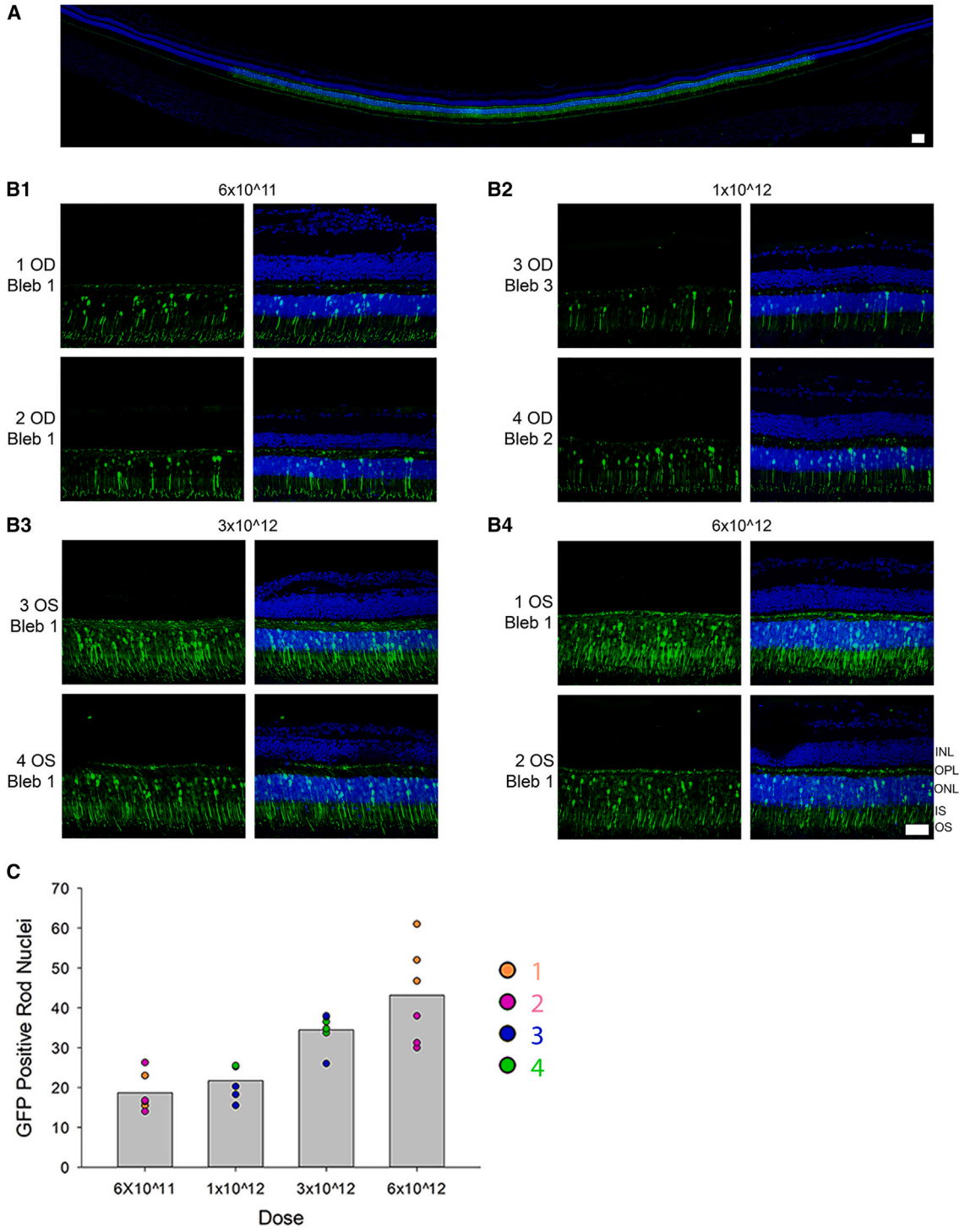

Figure 1. Reporter gene expression in nonhuman primates following subretinal injection

(A) Retinal section across injection bleb showing GFP expression (green) within the bleb. Blue is DAPI nuclear stain. Size bar, 100 μm. (B) Representative sections from blebs of the four dose groups (B1–B4). In each case, GFP expression (using anti-GFP antibody) is shown in green in the left panel, and GFP expression merged with DAPI (blue) is shown in the right panel. Doses (vector genomes) are indicated above each panel, and animal number, eye, and bleb imaged are indicated beside each panel. A dose effect is evident. Size bar, 50 μm. Key: INL, inner nuclear layer; OPL, outer plexiform layer; ONL, outer nuclear layer; IS, inner segment; OS, outer segment. (C) Comparative number of GFP expressing outer nuclear cell nuclei per unit length for each dose group, illustrating the dose effect. The color key indicates the individual animals.

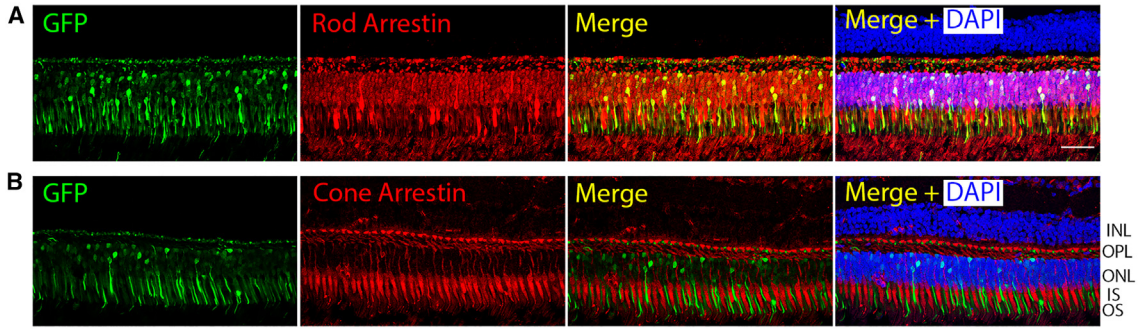

Figure 2. Representative IHC of NHP retinal sections showing exclusive rod transduction

(A) Panel illustrating the co-localization of GFP expression with rod arrestin. (B) Double labeling for GFP with cone arrestin showing that there is no detectable GFP expression in cone photoreceptors. Size bar, 50 μm. Key: INL, inner nuclear layer; OPL, outer plexiform layer; ONL, outer nuclear layer; IS, inner segment; OS, outer segment.

avoid a type II statistical error. Rod function was markedly improved in each treated eye for all four dose groups (Gp1–Gp4) as assessed by ERG (Figures 5, S5, and S6). The dark-adapted ERGs showed a lowering of response threshold (i.e., responses present to weaker flashes) by 1.5–2 log units for b-wave threshold (Figure S5), and amplitudes were increased compared with the untreated *CNGB1*-mutant dogs. The panel in Figure 5A shows recordings from a representative untreated eye from a 9-month-old dog compared with a treated eye at 6 and 12 months post treatment. In addition to the single-flash ERGs, the response to a 5-Hz flicker stimulus at a luminance that stimulates only rods was recorded (Figure 5B) and showed a similar improvement in function in the treated eyes. Bar graphs in Figures 5C–5E show the a- and b-wave amplitude improvements for the standard flashes recommended by the International Society for Clinical Electrophysiology of Vision (ISCEV), which are 0.01 cd·s/m^2 for a rod only response (only a b-wave is present at this stimulus strength) and 3 and 10 cd·s/m^2 (both a- and b-waves) for a "standard" and "strong" flash, both of which have rod and cone contributions. The red ERG tracings in Figure 5A are the tracings recorded in response to the ISCEV stimuli. Each treatment group showed a clear and statistically significant improvement in ERG amplitudes for each luminance indicative of rod functional rescue (Table S3). This was present at the 6-month PI time point and maintained in those dogs kept until 12 months PI (Figures 5C–5E) (note Gp1 dogs and three of the five Gp2 dogs were euthanized prior to the 12-month outcome measure time point). Tables S3 and S4 show the results of statistical analysis for each of the ISCEV recommended stimuli. The amplitude of the 5-Hz rod flicker response (Figure 5F) is also considerably improved following treatment (with a significant difference in mean amplitudes between each treatment group and untreated controls $p < 0.001$ F-test, linear mixed model). The increase in the ERG amplitudes at some luminances in the Gp2 dogs between 6- and 12-month timepoints is partly accounted for the fact that only two of the five dogs in this group were maintained until 12 months. The mean amplitudes for Gp3 animals are lower than the other groups. One animal in this group appeared to develop a mild inflammatory response that was initially detected on spectral domain optical coherence tomography (SD-OCT) examination as preretinal vitreous cells. Regions of focal retinal degeneration developed within the ventral portion of one of the treatment blebs (discussed further below). This dog had lower amplitude ERGs than others in the group but still showed evidence of rod rescue. The degree of rescue showed some within-group variance, which appeared, as would be expected, to correlate with the final size of the injection bleb (i.e., the area of the retina treated). There were significant differences between some of the amplitude measurements between some of the groups (see Table S4). Notably Gp4 amplitudes at 6 months PI were significantly greater than those of Gp3 dogs, but by 12 months PI, only the b-wave in response to the 0.01 cd s/m^2 luminance was significantly different between the two groups. Despite some differences between the groups, all groups showed marked improvement in rod function compared with the untreated *CNGB1*-mutant controls. Further analysis of rod function was achieved by modeling of the initial downslope of the rod-mediated a-wave, which provides a measure for maximal photoreceptor response (*Rmax*) and retinal sensitivity (S). A second method of using ERG data to assess retinal function and sensitivity was performed by modeling the first limb of the dark-adapted b-wave plotted against stimulus luminance (in normal animals, this is the result of rod function). This is known as the Naka-Rushton function and utilizes a Michaelis-Menten formula. Additional ERG measures from seven untreated young *CNGB1* mutant dogs were included in the statistical analysis to avoid a type II statistical error. Modeling of the dark-adapted rod a-wave (Figure S6) showed significant improvements in both Rmax of the treated eyes (Rmax of combined treated eyes = 41.4 ± 18.4 μV; untreated controls = 8.5 ± 6.2 μV mixed linear model F-test: $p = 5.44 \times 10^{-7}$) and in retinal sensitivity S (treated = 79.1 ± 29.7 1/[cd/m^2 s^3], untreated = 35.9 ± 22.3 1/[cd/m^2 s^3] mixed linear model F-test: $p = 3.49 \times 10^{-8}$). There was no difference in these parameters between the 6- and 12-month PI assessment times. Gp4 dogs had a significantly higher value for Rmax compared with the other treatment groups (data not shown). Otherwise, there was no significant difference in these parameters between treatment groups. Naka-Rushton fitting to the first limb of the dark-adapted b-wave amplitude versus luminance was used to provide a value for Vmax (maximum amplitude) and sensitivity S (stimulus strength required to produce a response amplitude of $^1/_2$ Vmax). For the statistical

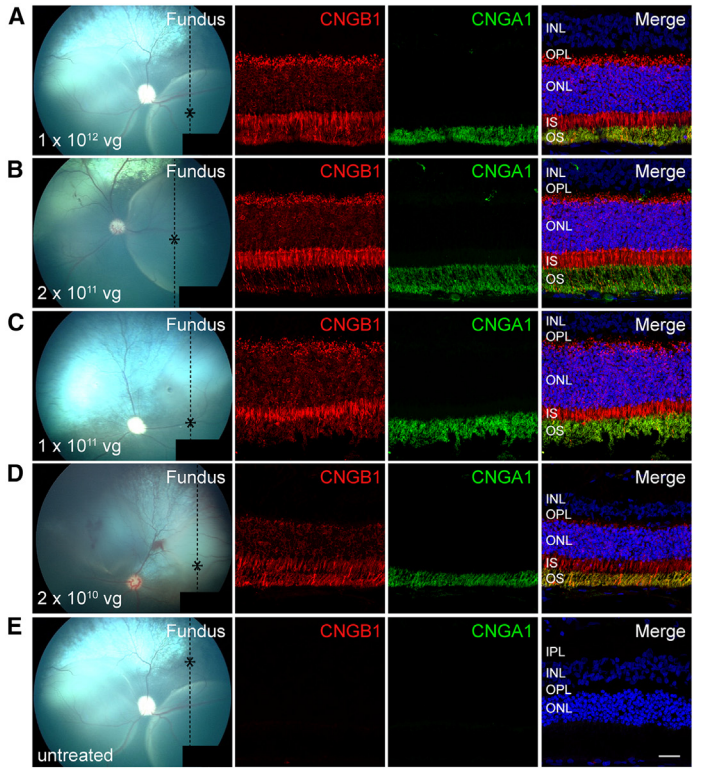

Figure 3. Montage showing retinal cross-sections from canine eyes from each treatment group from the highest to the lowest dose

(A) Dose group 4 (17-011 OD), (B) dose group 3 (17-007 OD), (C) dose group 2 (17-040 OD), and (D) dose group 1 (18-076 OS). (E) Untreated portion of a treated eye (17-011 OD). The first column is a color fundus image taken immediately after subretinal injection. The dotted line shows the plane of the histological section and the asterisk the region of the section imaged. The first IHC column is labeled for CNGB1 (in red) and shows a dosage effect. The next column shows CNGA1 labeling (in green) also showing a dosage effect. Note that CNGA1 expression is dependent on CNGB1 expression. The final column is the merge. Size bar, 25 μm.

analysis, results from five untreated age-matched *CNGB1* mutant dogs were used. The value of Vmax and S were both significantly improved in the treated eyes. Vmax at the 12-month time point mean of treated eyes was 65.8 ± 34.1 μV, and for untreated, it was 9.6 ± 7.7 μV (mixed linear model F-test: p = 0.015). For S at the 12-month time point, the mean of treated eyes was 0.013 ± 0.03 cd s/m^2 and untreated = 0.26 ± 0.21 cd s/m^2 (mixed linear model F-test: $p = 5.1 \times 10^{-7}$). The improvement in S reflects the left shift of the b-wave luminance response plots shown in Figure S5 showing the treated retina could respond to much lower luminance stimuli than the untreated retina.

Gene augmentation using AAV5-RHO-CNGB1 leads to preservation of cone function in the *CNGB1* dog model

CNGB1-mutant dogs have a relatively slow rod degeneration with a gradual secondary loss of cones. We analyzed the light-adapted (cone) ERG to see if the treated dogs had preservation of cone function. Figure S7 and Table S5 show the amplitudes of the a- and b-wave responses to the ISCEV standard flash amplitudes and the cone flicker (33-Hz) responses for the untreated control eyes (group 0 and breed and age-matched additional eyes to avoid a type II statistical error) and the treated eyes. These data were analyzed using a split-plot ANOVA with one grouping factor treatment and one repeat factor (time, 6 or 12 months PI). The mean amplitudes for a-wave, b-wave, and flicker were all significantly different between treated and control ($F(1, 18.2) = 20.69$ $p = 2.4 \times 10^{-4}$; $F(1, 18.4) = 11.9$, $p = 2.8 \times 10^{-3}$; $F(1, 19) = 7.2$, $p = 1.5 \times 10^{-2}$ respectively). The effect of time (6 months vs. 12 months PI) was not significant (data not shown).

To further investigate the cone responses, the Hood and Birch model for the cone a-wave was applied (Figure S7B).[18] This provides a measure of the maximal photoreceptor response (R_{mp3}). This was significantly higher in the treated groups (all groups combined) (11.03 ± 4.99 μV) compared with untreated controls (6.43 ± 2.74 μV) (mean ± SD) (mixed linear model F = 2.206, p = 0.027). Taken together, this analysis of cone ERG responses provides evidence of the preservation of cone function when rod rescue is achieved by gene augmentation therapy.

Gene augmentation using AAV5-RHO-CNGB1 restores rod-mediated vision in the *CNGB1* dog model

To show whether improved rod ERG function translated into improved rod-mediated vision, a previously described four-choice vision testing device was utilized. For each "run," one of the four exit tunnels is open. If the dog can see the open tunnel, it will exit through it. The exit choice and time to exit are recorded. As *CNGB1*-mutant dogs maintain cone-mediated vision for several years, results under scotopic conditions that test rod-mediated vision were analyzed. At these low light levels, untreated *CNGB1* dogs make mistakes in tunnel choice and are slow to exit. Unaffected wild-type dogs routinely choose the correct exit and will exit rapidly. Dogs of all treatment groups (Gp1–Gp4) chose the correct (open) tunnel nearly 100% of the time and exited the device rapidly (Figure 6). These results were statistically significant for each treatment group (see Table S6 for p values). For the dogs maintained until 12 months PI, the vision testing results were no different from those at 6 months PI. There was no difference in vision testing outcomes between the four treatment groups. Vision testing at mesopic and photopic levels showed there was no performance difference between treated and untreated dogs, both of which performed similarly to wild-type dogs, reflecting maintained cone vision at these ages (data not shown).

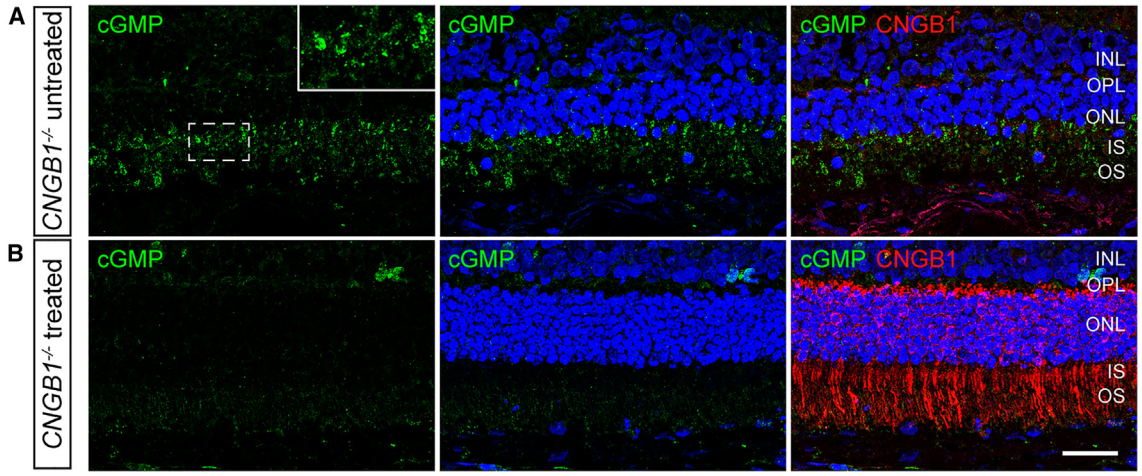

Figure 4. Gene augmentation therapy reverses disease-related cGMP accumulation

(A) shows an untreated retinal area of a *CNGB1* mutant dog (17-011 OD group 4). cGMP is in green with the insert showing a magnified view of the region in the white box. Note cGMP is detected in the inner and outer segment layers of the photoreceptors. (B) shows the same eye in a treated retinal region cGMP is green and CNGB1 red. Note the lack of accumulation of cGMP in the treated retinal region where CNGB1 labeling is present. Size bar, 25 μm.

Gene augmentation therapy using AAV5-RHO-CNGB1 preserves retinal structure in the *CNGB1* dog model

A comparison of retinal layer thicknesses (measured *in vivo* by SD-OCT) at 12 months post treatment (Gp 2, 3, and 4) was made between the treatment bleb and the adjacent untreated retina in the same eye showing outer retinal preservation in the treated eyes. Figure 7B2 shows a heatmap of a treatment bleb (Gp3 dog 17-007 OD lateral bleb) and clearly shows the preservation of total retinal thickness compared with the adjacent untreated retina. Figure 7C shows the ratio of thickness of the REC+ (measurement from outer plexiform layer to retinal pigment epithelium, representing the full length of the photoreceptors), outer nuclear layer, inner retina (ILM to inner nuclear layer), and total retinal layer thickness between regions within the bleb and adjacent retinal regions outside of the bleb. In all three treatment groups analyzed at 12 months post treatment, the outer retina was thicker in the treated region (REC+ and outer nuclear layer [ONL]) for all animals with the exception of one group 3 eye (17-010 OD) in which inflammation had developed in the injected eye (see below). The inner retina was very similar in thickness between regions, and the total retina was thicker in the treated region (this was primarily due to preservation of the outer retina). Figure 7D shows representation SD-OCT cross-sectional images of retina within the treatment bleb and the adjacent untreated region.

Adverse events in AAV5-RHO-CNGB1 treated dog eyes

The subretinal injections were generally well tolerated, and no adverse events noted in injected eyes except for one group 3 eye (17-010 OD). At the 3-month PI time point, vitreous cells were noted on OCT examination indicative of mild vitreal (or possibly vitreo-retinal) inflammation. A course of prednisone at a tapering dose (2 mg/kg) was instigated, and this appeared to suppress the inflammation. The eye still showed rescue of rod function with recordable rod ISCEV ERG response (which is absent in untreated eyes), although the amplitudes were lower than in other group 3 eyes. Vision testing also showed that treatment provided rod-mediated vision. However, circular patches of retinal and choroidal thinning developed at the lower region of the ventral bleb (Figure S8). The outer retinal measurements on SD-OCT for this eye showed some retinal thinning in the bleb compared with the adjacent non-treated region (see Figure 7C) in addition to the focal areas of complete loss. IHC showed that there remained *CNGB1* expression in the non-degenerated region of the bleb (Figures S4A and S4B).

DISCUSSION

There is an unmet need for a treatment for RP, and currently there is no curative treatment. *CNGB1*-RP has several features that make it an attractive target for gene augmentation therapy. Importantly, the affected patients lack rod function from an early age, allowing for potential early diagnosis, and despite the early onset, they have a slow loss of retinal structure as rods are gradually lost.[12] Cones do not express *CNGB1* and degenerate later in the disease process, following death of the surrounding supporting rods. The slow progression of the condition and the disconnect between loss of function and loss of structure gives the opportunity for early intervention while a population of potentially rescuable rod photoreceptors remain, and cone loss has not progressed. Relevant animal models (both mouse and dog) are established and can be used for development of translation therapy. The *CNGB1*-mutant dog utilized in the current study recapitulates many aspects of human *CNGB1*-RP, making it a particularly valuable model.[11,14]

One potential hurdle for AAV gene augmentation therapy of *CNGB1*-RP is that the size of *CNGB1* cDNA (3.76 kb) limits the amount of additional DNA that can be added to the AAV expression cassette without exceeding its packaging limit of 4.7 kb.[19] This leaves less than 1.0 kb space for additional sequences and, thus, prevents the use of common and well-established promoters for rod transduction and regulatory elements (e.g., a combination of bovine growth

Table 1. List of the dogs and details of the injected dose, eye, and follow-up times

Titer (vg/mL)	Total dose delivered (vg total)	Dog	Sex	Eye	Follow-up time points (months)	Time of euthanasia post injection (months)
Group 0–2 eyes untreated controls						
Nothing	nothing	17-038	F	left	6, 12	12
Nothing	nothing	17-042	F	left	6, 12	12
Group 1–3 eyes aav5-rho-cngb1 injected						
1E+11	2E+10	17-041	F	right	6	6
1E+11	2E+10	17-040	M	left	6	6
1E+11	2E+10	18-076	M	left	6	9
Group 2–5 eyes aav5-rho-cngb1 injected						
5E+11	1E+11	17-041	F	left	6	6
5E+11	1E+11	17-040	M	right	6	6
5E+11	1E+11	18-073	F	right	6, 12	kept long term
5E+11	1E+11	18-074	M	left	6, 12	kept long term
5E+11	1E+11	18-076	M	right	6	9
Group 3–5 eyes aav5-rho-cngb1 injected						
1E+12	2E+11	17-010	F	right	6, 12	12
1E+12	2E+11	17-011	M	left	6, 12	12
1E+12	2E+11	17-007	M	right	6, 12	12
1E+12	2E+11	17-038	F	right	6, 12	12
1E+12	2E+11	17-042	F	right	6, 12	12
Group 4–5 eyes aav5-rho-cngb1 injected						
5E+12	1E+12	17-010	F	left	6, 12	12
5E+12	1E+12	17-011	M	right	6, 12	12
5E+12	1E+12	17-007	M	left	6, 12	12
5E+12	1E+12	18-073	F	left	6, 12	kept long term
5E+12	1E+12	18-074	M	right	6, 12	kept long term

hormone polyA with the woodchuck stomatitis virus posttranscriptional regulatory element). In particular, use of the previously well-characterized 0.8-kb human rhodopsin promoter, which would be anticipated to be suitable to ensure strong and specific rod expression, would exceed the optimal packaging limit. In this study we showed that a <200-bp short version of the human rhodopsin promoter drives exclusive transgene expression in rod photoreceptors of three species: mouse, dog, and most importantly NHP. This makes it an excellent candidate for use in a translational construct. Our recent study in *Cngb1*$^{-/-}$ mice showed that this promoter could drive expression of the human *CNGB1* (hCNGB1) cDNA in murine rods and provide rescue of the phenotype.[15] Previous gene augmentation proof-of-principle studies in the dog model used a *GRK1* promoter to drive expression of the canine cDNA. While use of this vector resulted in robust rescue of rod function, *GRK1* can also drive transgene expression in cone photoreceptors, which is not desired for treatment of *CNGB1*-RP because *CNGB1* is not expressed in cones. In the current study, we were able to show convincing rod functional rescue and structural preservation in the dog model using this new translatable construct, which is an important step toward a human clinical trial.

The human CNGB1 protein resulting from transgene expression was able to combine with endogenous canine CNGA1 to form a functional CNG channel in the rod outer segment. IHC showed that treatment prevented degradation and restored trafficking of the active CNGA1 channel subunit to the outer segment, which is minimal in the absence of CNGB1.[20] The chimeric channel was functional, shown by the reversal of the accumulation of cGMP that occurs in rods in this model and restoration of a rod-mediated ERG as well as a substantial improvement in scotopic vision. Noticeable on IHC studies was the presence of the hCNGB1 protein within the entire rod cell body in addition to the outer segment within the treated retinal regions. In IHC of wild-type animals, CNGB1 is only detectable in rod outer segments.[11] The detection of hCNGB1 in the dog rod cell body and inner segment may indicate that at the vector doses used there was over-expression of the transgene, and indeed functional rescue was achieved at all doses tested in the current study. We noted that at the edge of the injection bleb, hCNGB1 was only detected in the rod outer segments (Figure S4). This suggests that as the dose of vector decreased, the accumulation of hCNGB1 in the cell body decreased accordingly. Human and canine CNGB1 proteins

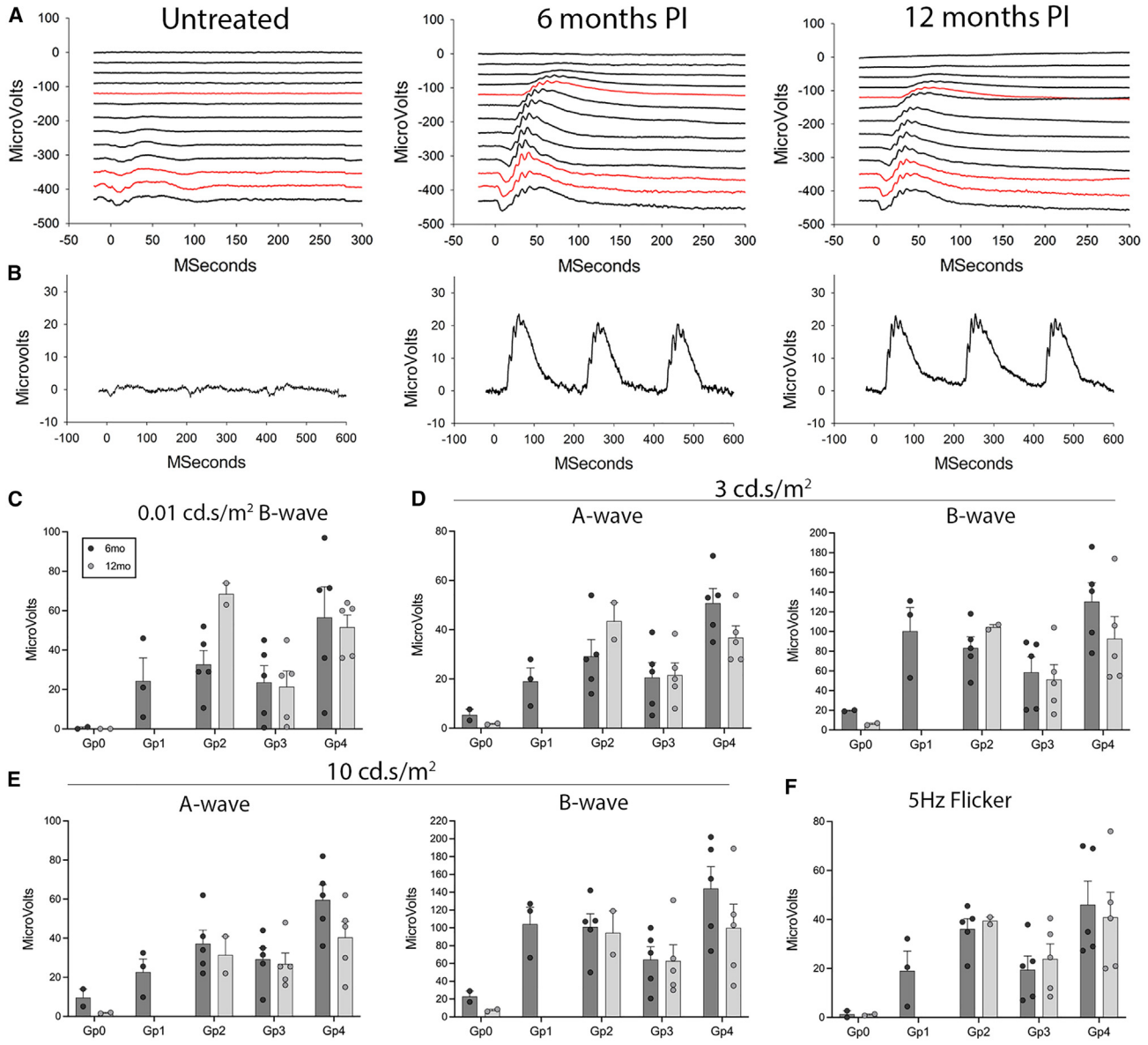

Figure 5. Gene augmentation rescue of rod function

(A) ERG dark-adapted luminance series from an untreated eye (17–042 OS 6 mo), an eye 6 months post injection (17-007 OD Gp3), and the same eye 12 months post injection. The red tracings indicate the ISCEV recommended ERG flash stimuli of 0.01, 3, and 10 cd·s/m^2. (B) Rod 5-Hz flicker (0.025 cd·s/m^2) results in the same eyes as in (A). (C–E) The mean (+/− SEM) dark-adapted ERG amplitudes for the ISCEV flash stimuli of 0.01, 3, and 10 cd·s/m^2 for the control eyes (Gp0) and the four dose groups (Gp1, Gp2, Gp3, Gp4). The 6-month post injection time point is in black, and the 12-month time point is in gray. Note that Gp1 was only maintained to 6 months post injection. There is no a-wave response at 0.01 cd·/m^2. (F) The mean (+/− SEM) 5-Hz rod flicker amplitudes for the same groups as in (C)–(E).

are not highly conserved at the N-terminus, the most notable difference being that the dog protein (NCBI Reference Sequence: NP_001271391.1) lacks a run of 42 residues making the full-length dog protein 1,209 AA vs. 1,251 AA for the human (NCBI Reference Sequence: NP_001288.3). This species difference in the protein may reduce the efficiency of trafficking to the outer segment as it is possible that hCNGB1 does not bind as efficiently to the canine CNGA1 as the wild-type canine protein does. Alternatively, excess hCNGB1 that does not pair with CNGA1 for trafficking to the outer segment might not be efficiently degraded in the dog rod photoreceptor and thus may accumulate. A similar accumulation in the inner segment was noted when the hCNGB1 was expressed in the *Cngb1*$^{-/-}$ mouse.[15] Despite the species protein differences, it is clear that the human:canine hybrid CNG channel provides excellent function, with the rod-mediated ERG amplitudes in the current study tending to be higher than those in our previous study using canine *CNGB1* driven by the

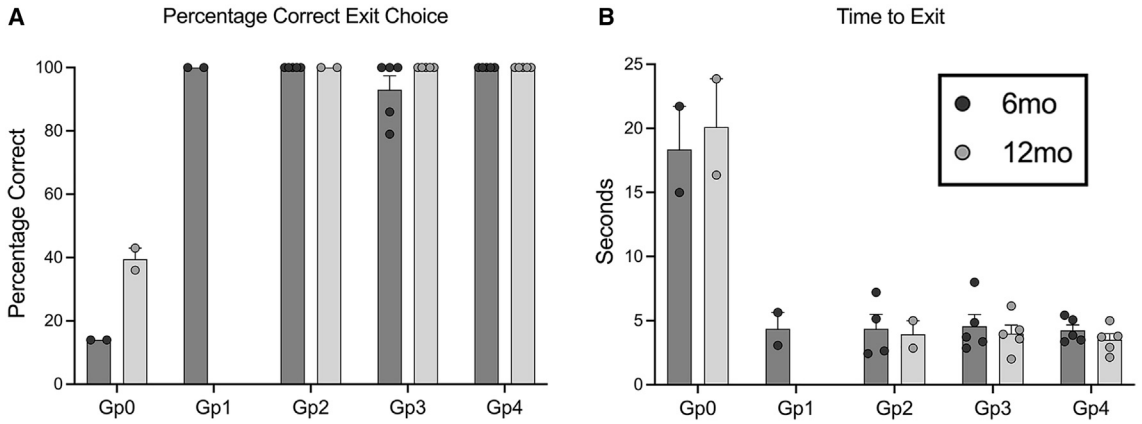

Figure 6. Vision testing. Scotopic vision of *CNGB1* mutant dogs restored by gene augmentation therapy

Vision testing outcome from four-choice vision testing device showing results under scotopic lighting levels (0.057 lux). (A) Shows mean (+/−SEM) percentage correct exit choices. (B) Mean (+/− SEM) time to exit. While the control dogs (GP0) fail to regularly choose the open exit and take a prolonged time to exit the device, dogs in all treated groups were able to identify the open exit accurately and rapidly exit the device. Gp1 dogs and two of the Gp2 dogs were only kept for 6 months so are not shown in the 12-month post-injection graphs.

GRK1 promoter.[14] Abnormal accumulation of human CNGB1 in the other parts of the cell body could lead to concerns of a toxic effect. This does not appear to occur over the long term with treatment effects staying stable over at least 12 months. One reason for this could be the fact that CNGB1-only channels are not able to support ion channel function.[21,22] Two animals are being followed for longer to see if rescue continues to be maintained. However, we did detect adverse effects in one Gp3 eye (dog 17-010 OD). Evidence of mild posterior segment inflammation was detected on SD-OCT examination at 3 months PI. This resolved with systemic steroids; however localized areas of degeneration developed toward the edge of the treatment bleb, and overall, there was some thinning of the outer retinal layers on SD-OCT measurement (Figures 7 and S8). Although showing rod rescue, this eye had lower ERG amplitudes than expected from the size of the subretinal injection blebs. Taken together, this could indicate that a lower dose of vector would be optimal to provide functional rescue without any risk of vector-induced toxicity. Gene-therapy-associated uveitis is becoming more widely recognized and can develop even if the administration is into the immune-privileged subretinal space. There are reports of similar perifoveal chorioretinal atrophy in patients treated for RPE65 Leber congenital amaurosis with FDA-approved AAV gene augmentation (Luxturna).[23,24]

Loss of *CNGB1* function results in a slowly progressive condition, as observed in dogs and in particular *CNGB1*-RP patients. It therefore takes a while before the preservation of retinal thickness becomes apparent. In all the treated eyes (with the exception of the eye that had inflammation), significant preservation of the outer retinal layers was apparent 12 months PI (Figure 7). In addition to preservation of retinal thickness, improvements in visualization of the reflective bands on SD-OCT that represent the photoreceptor inner and outer segment regions became apparent after intervention. This structural improvement was observable not only in the corresponding area before and after subretinal gene therapy but also in the comparison of treated to untreated regions within the injected eye. With a relatively slow degeneration, secondary loss of cone function is slow to develop. Analysis of cone ERGs showed that the treated eyes had preservation of cone ERG responses with a significant difference in amplitudes in the treated eyes being detected from as soon as 6 months PI (Figure S7). As cones do not express *CNGB1*, this shows that the rescue of rods has a beneficial effect on cones function and survival. Preservation of cone-mediated vision is a major aim of successful therapy for *CNGB1*-RP. Retinal preservation in the bleb areas was also apparent on IHC of retinal sections (Figure S2).

Further evidence to support the safety of AAV5 as a delivery vector was provided by the biodistribution study in NHPs with tissues collected at 3 months post dosing. The vector genome was not detected in any non-ocular tissues. Of the central visual pathways sampled, only one repeat sample of optic nerve in a single animal had detectable vector DNA.

In conclusion, the AAV5-RHO-CNGB1 vector tested in this project is a very promising translational candidate for a future human clinical trial addressing *CNGB1*-RP.

MATERIALS AND METHODS

Vector production

Vector production has been reported previously.[15] An AAV5 was packaged with a construct with a short human rhodopsin promoter driving expression of either enhanced green fluorescent protein (*eGFP*) for reporter gene studies or human *CNGB1* cDNA (for dog therapeutic studies).

Animals

All animal procedures were approved by the relevant Institutional Animal Care and Use Committee and adhered to the ARVO Statement for the Use of Animals in Ophthalmic and Vision Research.

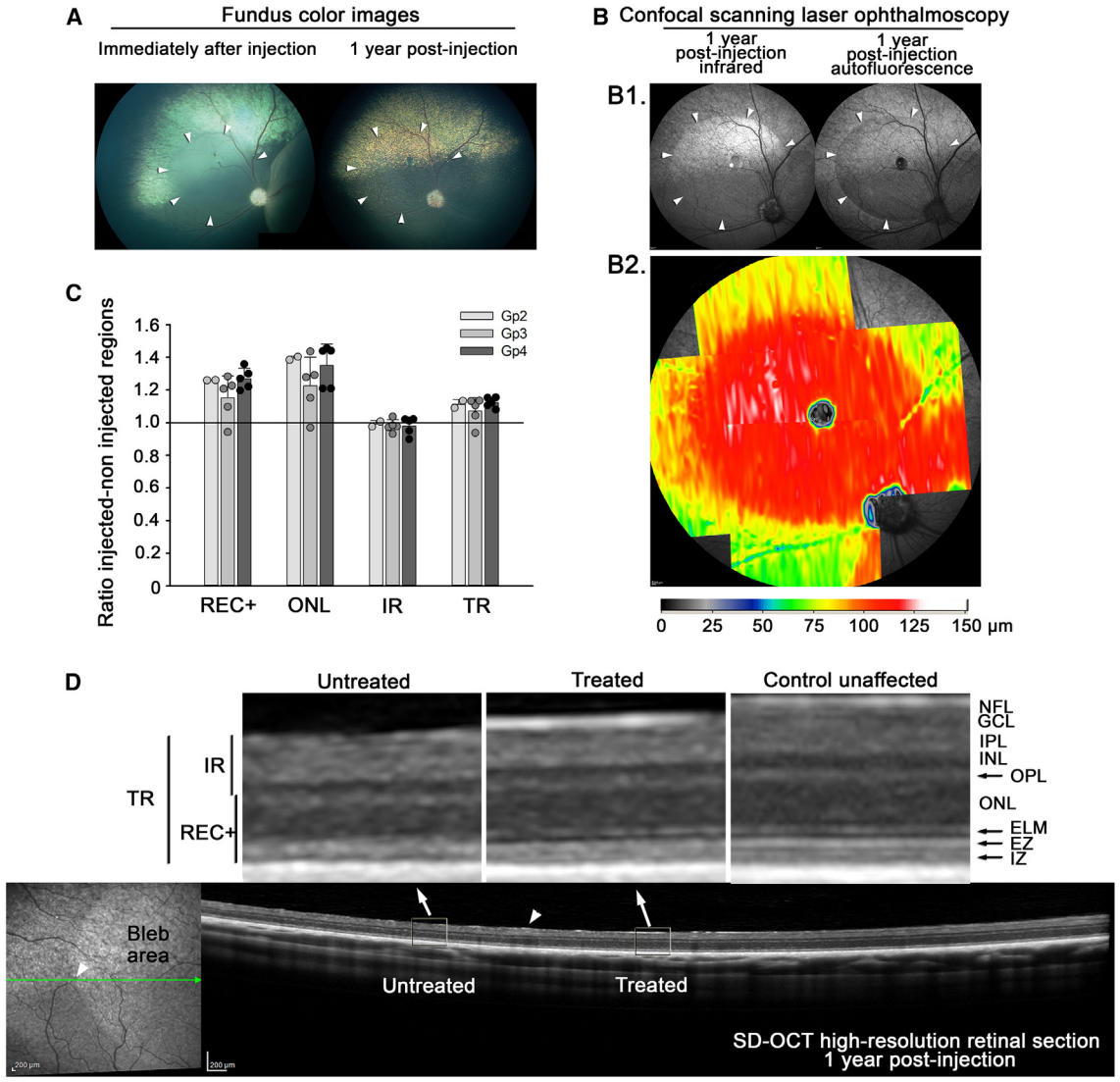

Figure 7. Structural preservation in treated eye

(A) Fundus photographs of Gp 3 (1E+12 Titer, 2E+11 Dose) dog 17-007 OD (right eye). The color fundus images show the injection bleb immediately after injection and then the fundus 1 year later. (B) B1. The cSLO images show infrared and autofluorescent imaging of the injected region. B2. A heatmap clearly shows the preservation of the treated retinal area, showing REC+ thickness. (C) REC+, ONL, IR, and TR thicknesses ratio of thickness in treated regions versus thickness in untreated regions at 12 months post injection for three doses/groups (mean ratio +/- SD). This shows preservation of the outer retina layers REC+ and ONL for all groups in the treated regions. (D) cSLO (left) and SD-OCT high-resolution retinal cross-section (right) images show the treated and untreated adjacent regions. The red arrow indicates the junction between treated and untreated regions. The two enlarged images above show high magnification of untreated and treated regions. Notice the thicker outer nuclear layer in the treated region and the improved definition of ELM, EZ, and IZ bands. TR, total retina; REC+, Receptor+; IR, inner retina; NFL, nerve fiber layer; GCL, ganglion cell layer; IPL, inner plexiform layer; INL, inner nuclear layer; OPL, outer plexiform layer; ONL, outer nuclear layer; ELM, external limiting membrane; EZ, ellipsoid zone; IZ, interdigitation zone.

All procedures concerning mice were reviewed and approved by a competent board appointed by the respective German government agency (Regierung von Oberbayern).

Nonhuman primates

Four rhesus macaque monkeys from the colony at the Oregon National Primate Research Center were used in the study to assess the efficacy and specificity of the vector capsid:promoter combination delivered by subretinal injection. They were maintained for 3 months PI undergoing regular clinical assessment and retinal imaging. After 3 months, they were euthanized, and the eyes were collected for frozen IHC, and a variety of tissues (Table S2) were collected for biodistribution studies.

Mice

Seven wild-type mice were used at Ludwig-Maximilians-University. The reporter gene construct was delivered by subretinal injection,

and the mice were maintained for 8 weeks. They underwent retinal imaging every 2 weeks to monitor green fluorescent protein (GFP) expression. After 8 weeks, mice were euthanized, and the eyes were processed for frozen IHC.

Dogs

Ten 3-month-old dogs from a colony of *CNGB1* mutant dogs were used in the study to assess phenotype rescue achieved by subretinal administration of the therapeutic vector. One wild-type dog was used to test the reporter gene construct.

Subretinal injections

Subretinal injections in NHPs were performed by a vitreoretinal surgeon via a standard pars plana transvitreal approach without vitrectomy as previously described[25] except that three smaller blebs (of ~30 μL) were made surrounding the fovea but without detaching the fovea. Two eyes each received one of four vector doses: 6.0E+11, 1.0E+12, 3.0E+12, and 6.0E+12, with the distribution among animals shown in Table S1.

Subretinal injections in mice were performed using a transscleral approach as previously described.[15]

Subretinal injections in dogs were performed via a standard pars plana transvitreal approach without vitrectomy as previously described[26] except that the aim was to produce two large subretinal blebs in the central fundus, one nasal and the other temporal to the optic disc. Fundus images were taken immediately after the injection using a video fundus camera (RetCam II, Clarity Medical Systems, Pleasanton, CA. USA).

In vivo retinal imaging

For NHPs, retinal imaging was performed prior to subretinal injection and at 1, 2, and 3 months PI under anesthesia with isoflurane vaporized in 100% oxygen. Imaging modes included standard color (Zeiss FF450, Oberkochen, Germany) and ultra-widefield red-green imaging (Optos California, Optos, Marlborough, MA); SD-OCT (Spectralis OCT, Heidelberg Engineering, Heidelberg, Germany); quantitative fluorescence imaging (Heidelberg Spectralis, BluePeak mode) done as previously described[27] with the addition of an internal fluorescence reference; and ultra-widefield autofluorescence imaging (Optos).

Mouse fundus images were recorded using an adapted Spectralis HRA+OCT diagnostic imaging platform (Heidelberg Engineering, Heidelberg, Germany) in combination with optic lenses as described previously.[28,29] Mice were anesthetized, and pupils were dilated as described before. To keep eyes moist, hydroxypropyl methylcellulose (Methocel 2%; OmniVision, Puchheim, Germany) and a corneal contact lens were applied on both eyes before mice were positioned in front of the retinal image lens. Fluorescent fundus images were acquired using the eGFP filter settings and analyzed using the Heidelberg Eye Explorer software V1.7.0.0 (Heidelberg Engineering, Heidelberg, Germany).

For dogs, wide-angle color fundus images were obtained using a RetCam II video fundus camera (Clarity Medical Systems, Pleasanton, CA, USA). Confocal scanning laser ophthalmoscopy (cSLO) and SD-OCT imaging (Spectralis HRA + OCT; Heidelberg Engineering, Heidelberg, Germany) were performed under general anesthesia, as previously described.[30,31] Single lines and volume scans were performed across the fundus, especially in the treated and adjacent untreated regions as described previously.[31] Total retinal (TR) thickness, thickness of the Receptor+ (REC+) layer (representative measure of the total length of the photoreceptor from the interdigitation zone, which is the interface of retinal pigment epithelium with the outer segments, to the outer plexiform layer), thickness of the ONL, and thickness of the inner retina (IR) were measured as previously described.[31] To compare retinal layer thicknesses between treated and untreated regions, measurements using the integrated Heidelberg Eye Explorer (HEYEX) software were performed for the treated retina 1,000 μm from the edge of the bleb, and an adjacent nontreated region was measured within 1,000 μm outside the bleb. The bleb and immediately outside the bleb in three treated – nontreated regions for each bleb. More precisely, the edge of each bleb was localized; then measurements of four layers were performed 1,000 μm inside and outside of the bleb (Figure S9 illustrates this protocol). Three paired measurements per bleb were obtained, and an average ratio between the adjacent treated and non-treated retinal regions per eye was calculated.

Retinal layer thickness color "heat maps" to give a clear representation of retinal layer thickness preservation were prepared using the HEYEX software, as previously described.[32]

Electroretinography (dogs)

ERG in dogs was performed as previously described.[31,33] This consisted of a dark-adapted series of increasing flash luminances from below b-wave threshold to a strong stimulus followed by a 5-Hz rod flicker. After 10 min light adaptation (at 30 cd/m^2), light-adapted single-flash and flicker (33-Hz) responses were recorded. ERG response amplitudes were measured in a standard fashion: a-wave amplitude from baseline to trough of a-wave and the b-wave from a-wave trough to peak of the b-wave that underlies the oscillatory potentials.[34] To further investigate rod photoreceptor function, the following equation described by Birch and Hood[35,36] was fit to the leading edge of the rod a-wave (after subtraction of the matched photopic waveform to remove cone contributions) as previously described.[37]

$$R(I,t)=(1-\exp[-I\cdot S\cdot(t-td)^2])\cdot R_{max} \text{ for } t>t_d$$

The amplitude R is a function of the retinal luminance I and time t after the flash, and t_d is a brief delay. S is a sensitivity factor, and R_{max} is the maximum amplitude of the response.

To assess retinal sensitivity, we also utilized Naka-Rushton fit to the first limb of the dark-adapted b-wave luminance response plot[38]:

$$R/V_m = L^n/(L^n+K^n)$$

V_m represents the maximum response amplitude of the first limb of the b-wave luminance:response plot, K is a semi-saturation constant considered a measure of retinal sensitivity, and n is dependent on the slope of the plot at the position of K, which may reflect retinal homogeneity.[39,40]

To further investigate cone function, we fit the following equation described by Hood and Birch to the leading edge of the cone a-wave as previously described.[37]

$$R(I,t)=(I \cdot S_c \cdot (t-t_d)^3)/(I \cdot S_c \cdot (t-t_d)^3 + 1) \cdot R_{mp3} \text{ for } t>t_d$$

The amplitude R is a function of the retinal luminance I and time t after the flash, and t_d is a brief delay. S_c is a sensitivity factor, and R_{mp3} is the maximum amplitude of the response.

Vision testing (dogs)

Assessment of vision was performed using a custom four-choice device previously developed and utilized.[41,42] This device consisted of a box with four exit tunnels. For each "trial run," the end of only one tunnel was open, this tunnel being randomly selected. The first tunnel entered was noted as the "exit choice," and the time to exit the tunnel was recorded. A series of seven lighting levels were used from bright room light down to a dim light that tests rod-mediated vision in dogs. Thus, a range of scotopic, mesopic, and photopic vision was tested. Each eye was tested separately by fitting an opaque contact lens in the contralateral eye. Fourteen repeat "trial runs" were performed at each light level for each eye, allowing the mean correct exit choice and mean exit times to be calculated.

Immunohistochemistry of retinal sections

Rhesus macaque eyes were immersion-fixed for 24 h in 4% paraformaldehyde. The anterior chamber was dissected off, and the remaining posterior eye cups were cryoprotected using 10%, 20%, and 30% sucrose concentrations. Samples were embedded horizontally in optimal cutting temperature compound blocks, frozen, and cut at 14-μm-thick sections using a Leica CM1850 cryostat. Slides used for immunofluorescence staining were dried and incubated for 30 min in a phosphate buffered saline-based blocking buffer containing 4% horse serum, 0.5% Triton X-100, and 1.0% bovine serum albumin. Antibodies used are listed in Table S7. Sections were incubated with the primary antibodies overnight at 4°C followed by the appropriate secondary Alexa-Fluor antibodies (1:300, Invitrogen, Carlsbad, CA, USA). Anti-GFP antibody was used to enhance the fluorescent signal of GFP generated from transgenic expression in retinal tissue. Retinal nuclei were counterstained using 4′,6-diamidino-2-phenylindole (DAPI) and cover-slipped with Fluoromount G (Southern Biotech). Confocal z stack images were acquired from retinal sections with 20x and 40x objectives using a Leica SP5 laser-scanning confocal microscope (Leica, Wetzlar, Germany).

Preparation of mouse eyes for IHC was performed as previously described.[29,43,44] Antibodies used are shown in Table S7.

Dog eyes were prepared for IHC as previously described.[45,46] Antibodies used are shown in Table S7.

Quantification of transduced rod photoreceptors in NHPs

For each eye, four representative 40x confocal images through the center of each bleb were acquired with constant laser intensity settings for GFP fluorescence. Color images were extracted from .lif files using ImageJ software and converted to 8-bit grayscale images. A lower threshold value limit of 90 pixels and upper value limit of 255 pixels was set for each z stack image in the GFP channel. Thresholded values (displayed in red) localized specifically to rod nuclei within the ONL were counted for the entire 40x image, representing a section of retina of 388 μM. Total counts are presented as number of GFP-positive nuclei per unit length.

Tissue biodistribution studies in NHPs

Assays were performed at the Powell Gene Therapy Center, University of Florida. DNA was extracted from tissues, anterior chamber fluid, and vitreous samples using a DNeasy Blood and Tissue kit (Qiagen, Venlo, Netherlands) according to the manufacturer's protocol and in-house standard operating procedures. DNA was quantified using the Quant-iT PicoGreen dsDNA Assay Kits (Invitrogen, Carlsbad, CA, USA) on a Synergy LX multimode microplate reader (BioTek, Winoosi, Vermont, USA). TaqMan quantitative PCR was performed on a QuantStudio 3 (Applied Biosystems, Foster City, CA, USA) using the QuantStudio Design and Analysis Software v1.4.1 (Applied Biosystems, Foster City, CA, USA) according to manufacturer's instructions. A primer and probe set was designed to the GFP gene of interest. Briefly, an 8-log standard curve covering a range of 1E+8 through 1E+0 copies was generated from a stock plasmid containing the GFP gene of interest (Aldevron, Fargo, ND USA), and Ct values for each standard were plotted against the log concentration of copies per sample. The linear regression of the resultant plot was utilized to calculate the copies within each sample. Each sample was tested in triplicate, with one replicate containing 10 copies of the target plasmid spiked in to test for inhibition of the reaction. Each 50-μL reaction contained 25 μL of TaqMan Universal PCR Master Mix (Applied Biosystems, Foster City, CA, USA), up to 0.1 μg of sample DNA, 700 nM of the forward and reverse primers, and 100 nM of fluorescein amidite (FAM)-labeled probe. Cycling followed manufacturer recommended guidelines, 5 min at 95°C for initial denaturation and enzyme activation, followed by 45 cycles altering between a 15-s period at 95°C for denaturing and a 60-s period at 60°C for annealing and extension. Results were averaged across two replicates and normalized to vector genome copies per μg DNA (vgc/μg DNA), and values less than 100 vector genome copies (vgc)/μg DNA were reported as below the lower limit of quantification.

GFP Forward: 5′-TTTCAAAGATGACGGGAACTACAA-3′

GFP Reverse: 5′-TCAATGCCCTTCAGCTCGAT-3′

GFP Probe: 6FAM-CCCGCGCTGAAGTCAAGTTCGAAG-TAMRA.

Statistical analysis

Analysis for a dose effect of GFP expression levels in NHP rods was assessed by a Welsch's one-way ANOVA. For most ERG and vision testing measures, variables were tested for homoscedasticity using the Breusch-Pagan test and for normality using the Shapiro-Wilks test, prior to calculation of the F-statistic using the F-test of the linear mixed effects model (LME).

To account for the repeated measures in the data, an LME model was employed utilizing the Statsmodels package in Python to examine statistical significance between groups serial ERGs performed in dogs following gene augmentation therapy fitting the following equation:

$$Y_{ij} = \beta_0 + \beta_1 X_{ij} + \gamma_i + \varepsilon_{ij}$$

Y_{ij} is the j^{th} measured response for subject i, X_{ij} is the covariate for this response, γ_i is the random effects parameter for subject i, and ε_{ij} is the error parameter for this response. β_0 and β_1 are fixed effect parameters for all subjects, corresponding to intercept and slope, respectively, and they are fit according to the restricted maximum likelihood optimized with the Broyden-Fletcher-Goldfarb-Shanno algorithm.[47]

Cone ERG amplitudes were compared with a split-plot ANOVA.

DATA AND MATERIALS AVAILABILITY

Data and materials supporting the findings of this manuscript are available from the corresponding authors upon reasonable request.

SUPPLEMENTAL INFORMATION

Supplemental information can be found online at https://doi.org/10.1016/j.ymthe.2023.04.005.

ACKNOWLEDGMENTS

Funded by NIH grants R24EY027285 to S.M.P.J., S.M., S.H.T., and W.W.H.; P51OD011092 and S10RR024585 to the Oregon National Primate Research Center (ONPRC). Also from Sanofi (to S.M.) and Myers-Dunlap Endowment to S.M.P.J. We thank Dr. Joe Hauptman for statistical analysis, Dr. Clay Smith (University of Florida) for rod and cone arrestin antibodies, Dr. Wolfgang Baehr (University of Utah) for a cone arrestin antibody, Dr. HWM Steinbusch (Maastricht University Medical Center) for the cGMP antibody, and Dr. Hammer Ammer (Ludwig-Maximilians-Universität München, Munich) for help with the design and generation of the CNGA1 antibody.

AUTHOR CONTRIBUTIONS

S.M.P.J. and S.M. conceptualized the studies with input from W.W.H., S.H.T., C.R.O., and A.F. S.M.P.J., L.M.O., N.P., J.Q., P.A.W., K.S., and L.F.L.P.M. performed the dog studies. J.S., L.M.R., R.R., A.L., T.J.M., and M.N. performed the primate studies. L.Z., J.W., and S.M. performed the mice studies and mouse and dog IHC. S.H.T. and W.W.H. reviewed the study. S.M.P.J., L.M.O., and L.Z. wrote the manuscript. All authors reviewed and edited the manuscript.

DECLARATION OF INTERESTS

C.R.O. and A.F. are employees of Sanofi. S.M. is listed as inventor on the patent application WO2018172961A1 "Gene therapy for the treatment of cngb1-linked retinitis pigmentosa" and is co-founder of the gene therapy company ViGeneron GmbH.

REFERENCES

1. Russell, S., Bennett, J., Wellman, J.A., Chung, D.C., Yu, Z.F., Tillman, A., Wittes, J., Pappas, J., Elci, O., McCague, S., et al. (2017). Efficacy and safety of voretigene neparvovec (AAV2-hRPE65v2) in patients with RPE65-mediated inherited retinal dystrophy: a randomised, controlled, open-label, phase 3 trial. Lancet *390*, 849–860.
2. Georgiou, M., Fujinami, K., and Michaelides, M. (2021). Inherited retinal diseases: therapeutics, clinical trials and end points-A review. Clin. Exp. Ophthalmol. *49*, 270–288.
3. Daiger, S.P., Rossiter, B.J.F., Greenberg, J., Christoffels, A., and Hide, W. (1998). Data services and software for identifying genes and mutations causing retinal degeneration. Invest. Ophthalmol. Vis. Sci. *39*, S295.
4. Hartong, D.T., Berson, E.L., and Dryja, T.P. (2006). Retinitis pigmentosa. Lancet *368*, 1795–1809.
5. Bareil, C., Hamel, C.P., Delague, V., Arnaud, B., Demaille, J., and Claustres, M. (2001). Segregation of a mutation in CNGB1 encoding the beta-subunit of the rod cGMP-gated channel in a family with autosomal recessive retinitis pigmentosa. Hum. Genet. *108*, 328–334.
6. Kondo, H., Qin, M., Mizota, A., Kondo, M., Hayashi, H., Hayashi, K., Oshima, K., Tahira, T., and Hayashi, K. (2004). A homozygosity-based search for mutations in patients with autosomal recessive retinitis pigmentosa, using microsatellite markers. Invest. Ophthalmol. Vis. Sci. *45*, 4433–4439.
7. Nassisi, M., Smirnov, V.M., Solis Hernandez, C., Mohand-Saïd, S., Condroyer, C., Antonio, A., Kühlewein, L., Kempf, M., Kohl, S., Wissinger, B., et al. (2021). CNGB1-related rod-cone dystrophy: a mutation review and update. Hum. Mutat. *42*, 641–666.
8. Hanany, M., Rivolta, C., and Sharon, D. (2020). Worldwide carrier frequency and genetic prevalence of autosomal recessive inherited retinal diseases. Proc. Natl. Acad. Sci. USA *117*, 2710–2716.
9. Zhong, H., Molday, L.L., Molday, R.S., and Yau, K.W. (2002). The heteromeric cyclic nucleotide-gated channel adopts a 3A:1B stoichiometry. Nature *420*, 193–198.
10. Hüttl, S., Michalakis, S., Seeliger, M., Luo, D.G., Acar, N., Geiger, H., Hudl, K., Mader, R., Haverkamp, S., Moser, M., et al. (2005). Impaired channel targeting and retinal degeneration in mice lacking the cyclic nucleotide-gated channel subunit CNGB1. J. Neurosci. *25*, 130–138.
11. Winkler, P.A., Ekenstedt, K.J., Occelli, L.M., Frattaroli, A.V., Bartoe, J.T., Venta, P.J., and Petersen-Jones, S.M. (2013). A large animal model for *CNGB1* autosomal recessive retinitis pigmentosa. PLoS One *8*, e72229.
12. Hull, S., Attanasio, M., Arno, G., Carss, K., Robson, A.G., Thompson, D.A., Plagnol, V., Michaelides, M., Holder, G.E., Henderson, R.H., et al. (2017). Clinical characterization of CNGB1-related autosomal recessive retinitis pigmentosa. JAMA Ophthalmol. *135*, 137–144.
13. Koch, S., Sothilingam, V., Garcia Garrido, M., Tanimoto, N., Becirovic, E., Koch, F., Seide, C., Beck, S.C., Seeliger, M.W., Biel, M., et al. (2012). Gene therapy restores vision and delays degeneration in the CNGB1(-/-) mouse model of retinitis pigmentosa. Hum. Mol. Genet. *21*, 4486–4496.
14. Petersen-Jones, S.M., Occelli, L.M., Winkler, P.A., Lee, W., Sparrow, J.R., Tsukikawa, M., Boye, S.L., Chiodo, V., Capasso, J.E., Becirovic, E., et al. (2018). Patients and animal models of CNGbeta1-deficient retinitis pigmentosa support gene augmentation approach. J. Clin. Invest. *128*, 190–206.
15. Wagner, J.E., Zobel, L., Gerhardt, M.J., O'Riordan, C.R., Frederick, A., Petersen-Jones, S.M., Biel, M., and Michalakis, S. (2021). In vivo potency testing of subretinal rAAV5.hCNGB1 gene therapy in the Cngb1 knockout mouse model of retinitis pigmentosa. Hum. Gene Ther. *32*, 1158–1170.
16. Maguire, A.M., High, K.A., Auricchio, A., Wright, J.F., Pierce, E.A., Testa, F., Mingozzi, F., Bennicelli, J.L., Ying, G.S., Rossi, S., et al. (2009). Age-dependent effects

of RPE65 gene therapy for Leber's congenital amaurosis: a phase 1 dose-escalation trial. Lancet *374*, 1597–1605.

17. Ochakovski, G.A., Bartz-Schmidt, K.U., and Fischer, M.D. (2017). Retinal gene therapy: surgical vector delivery in the translation to clinical trials. Front. Neurosci. *11*, 174.
18. Hood, D.C., and Birch, D.G. (1995). Phototransduction in human cones measured using the alpha-wave of the ERG. Vis. Res. *35*, 2801–2810.
19. Wu, Z., Yang, H., and Colosi, P. (2010). Effect of genome size on AAV vector packaging. Mol. Ther. *18*, 80–86.
20. Petersen-Jones, S.M., Pasmanter, N., Occelli, L.M., Querubin, J.R., and Winkler, P.A. (2022). Residual rod function in CNGB1 mutant dogs. Doc. Ophthalmol. *145*, 237–246.
21. Xue, J., Han, Y., Zeng, W., and Jiang, Y. (2022). Structural mechanisms of assembly, permeation, gating, and pharmacology of native human rod CNG channel. Neuron *110*, 86–95.e5.
22. Barret, D.C.A., Schertler, G.F.X., Kaupp, U.B., and Marino, J. (2022). The structure of the native CNGA1/CNGB1 CNG channel from bovine retinal rods. Nat. Struct. Mol. Biol. *29*, 32–39.
23. Reichel, F.F., Seitz, I., Wozar, F., Dimopoulos, S., Jung, R., Kempf, M., Kohl, S., Kortüm, F.C., Ott, S., Pohl, L., et al. (2022). Development of retinal atrophy after subretinal gene therapy with voretigene neparvovec. Br. J. Ophthalmol.. bjophthalmol-2021-321023.
24. Gange, W.S., Sisk, R.A., Besirli, C.G., Lee, T.C., Havunjian, M., Schwartz, H., Borchert, M., Sengillo, J.D., Mendoza, C., Berrocal, A.M., et al. (2022). Perifoveal chorioretinal atrophy after subretinal voretigene neparvovec-rzyl for RPE65-mediated leber congenital amaurosis. Ophthalmol. Retina *6*, 58–64.
25. Simpson, E.M., Korecki, A.J., Fornes, O., McGill, T.J., Cueva-Vargas, J.L., Agostinone, J., Farkas, R.A., Hickmott, J.W., Lam, S.L., Mathelier, A., et al. (2019). New MiniPromoter Ple345 (NEFL) drives strong and specific expression in retinal ganglion cells of mouse and primate retina. Hum. Gene Ther. *30*, 257–272.
26. Petersen-Jones, S.M., Bartoe, J.T., Fischer, A.J., Scott, M., Boye, S.L., Chiodo, V., and Hauswirth, W.W. (2009). AAV retinal transduction in a large animal model species: comparison of a self-complementary AAV2/5 with a single-stranded AAV2/5 vector. Mol. Vis. *15*, 1835–1842.
27. McGill, T.J., Renner, L.M., and Neuringer, M. (2016). Elevated fundus autofluorescence in monkeys deficient in lutein, zeaxanthin, and omega-3 fatty acids. Invest. Ophthalmol. Vis. Sci. *57*, 1361–1369.
28. Mühlfriedel, R., Michalakis, S., Garrido, M.G., Sothilingam, V., Schön, C., Biel, M., and Seeliger, M.W. (2019). Optimized subretinal injection technique for gene therapy approaches. Methods Mol. Biol. *1834*, 405–412.
29. Schön, C., Asteriti, S., Koch, S., Sothilingam, V., Garcia Garrido, M., Tanimoto, N., Herms, J., Seeliger, M.W., Cangiano, L., Biel, M., et al. (2016). Loss of HCN1 enhances disease progression in mouse models of CNG channel-linked retinitis pigmentosa and achromatopsia. Hum. Mol. Genet. *25*, 1165–1175.
30. Mowat, F.M., Gervais, K.J., Occelli, L.M., Annear, M.J., Querubin, J., Bainbridge, J.W., Smith, A.J., Ali, R.R., and Petersen-Jones, S.M. (2017). Early-onset progressive degeneration of the area centralis in RPE65-deficient dogs. Invest. Ophthalmol. Vis. Sci. *58*, 3268–3277.
31. Occelli, L.M., Schön, C., Seeliger, M.W., Biel, M., Michalakis, S., and Petersen-Jones, S.M. (2017). Gene supplementation rescues rod function and preserves photoreceptor and retinal morphology in dogs, leading the way toward treating human PDE6A-retinitis pigmentosa. Hum. Gene Ther. *28*, 1189–1201.
32. Occelli, L.M., Tran, N.M., Narfström, K., Chen, S., and Petersen-Jones, S.M. (2016). CrxRdy cat: a large animal model for CRX-associated leber congenital amaurosis. Invest. Ophthalmol. Vis. Sci. *57*, 3780–3792.
33. Annear, M.J., Bartoe, J.T., Barker, S.E., Smith, A.J., Curran, P.G., Bainbridge, J.W., Ali, R.R., and Petersen-Jones, S.M. (2011). Gene therapy in the second eye of RPE65-deficient dogs improves retinal function. Gene Ther. *18*, 53–61.
34. Pasmanter, N., and Petersen-Jones, S.M. (2020). A review of electroretinography waveforms and models and their application in the dog. Vet. Ophthalmol. *23*, 418–435. https://doi.org/10.1111/vop.12759.
35. Hood, D.C., and Birch, D.G. (1990). The A-wave of the human electroretinogram and rod receptor function. Invest. Ophthalmol. Vis. Sci. *31*, 2070–2081.
36. Hood, D.C., and Birch, D.G. (1996). Assessing abnormal rod photoreceptor activity with the a-wave of the electroretinogram: applications and methods. Doc. Ophthalmol. *92*, 253–267.
37. Pasmanter, N., Occelli, L.M., and Petersen-Jones, S.M. (2021). ERG assessment of altered retinal function in canine models of retinitis pigmentosa and monitoring of response to translatable gene augmentation therapy. Doc. Ophthalmol. *143*, 171–184.
38. Robson, J.G., Maeda, H., Saszik, S.M., and Frishman, L.J. (2004). In vivo studies of signaling in rod pathways of the mouse using the electroretinogram. Vis. Res. *44*, 3253–3268.
39. Naka, K.I., and Rushton, W.A. (1966). S-potentials from colour units in the retina of fish (Cyprinidae). J. Physiol. *185*, 536–555.
40. Evans, L.S., Peachey, N.S., and Marchese, A.L. (1993). Comparison of three methods of estimating the parameters of the Naka-Rushton equation. Doc. Ophthalmol. *84*, 19–30.
41. Gearhart, P.M., Gearhart, C.C., and Petersen-Jones, S.M. (2008). A novel method for objective vision testing in canine models of inherited retinal disease. Invest. Ophthalmol. Vis. Sci. *49*, 3568–3576.
42. Annear, M.J., Gornik, K.R., Venturi, F.L., Hauptman, J.G., Bartoe, J.T., and Petersen-Jones, S.M. (2013). Reproducibility of an objective four-choice canine vision testing technique that assesses vision at differing light intensities. Vet. Ophthalmol. *16*, 324–328.
43. Michalakis, S., Mühlfriedel, R., Tanimoto, N., Krishnamoorthy, V., Koch, S., Fischer, M.D., Becirovic, E., Bai, L., Huber, G., Beck, S.C., et al. (2010). Restoration of cone vision in the CNGA3-/- mouse model of congenital complete lack of cone photoreceptor function. Mol. Ther. *18*, 2057–2063.
44. Michalakis, S., Geiger, H., Haverkamp, S., Hofmann, F., Gerstner, A., and Biel, M. (2005). Impaired opsin targeting and cone photoreceptor migration in the retina of mice lacking the cyclic nucleotide-gated channel CNGA3. Invest. Ophthalmol. Vis. Sci. *46*, 1516–1524.
45. Mowat, F.M., Breuwer, A.R., Bartoe, J.T., Annear, M.J., Zhang, Z., Smith, A.J., Bainbridge, J.W.B., Petersen-Jones, S.M., and Ali, R.R. (2013). RPE65 gene therapy slows cone loss in Rpe65-deficient dogs. Gene Ther. *20*, 545–555.
46. Mowat, F.M., Gornik, K.R., Dinculescu, A., Boye, S.L., Hauswirth, W.W., Petersen-Jones, S.M., and Bartoe, J.T. (2014). Tyrosine capsid-mutant AAV vectors for gene delivery to the canine retina from a subretinal or intravitreal approach. Gene Ther. *21*, 96–105.
47. Seabold, S., and Perktold, J. (2010). Statsmodels: econometric and statistical modeling with python. In Proceedings of the 9th Python in Science Conference, *57* (Scipy), p. 61.